First-order reflection/transmission coefficients for unconverted plane P waves in weakly anisotropic media

Véronique Farra [1] and Ivan Pšenčík [2]

[1] *Institut de Physique du Globe de Paris*, 4 *Place Jussieu*, 75252 *Paris Cedex* 05, *France. E-mail: farra@ipgp.fr*
[2] *Institute of Geophysics, Acad. Sci. of Czech Republic, Boční II*, 141 31 *Praha* 4, *Czech Republic. E-mail: ip@ig.cas.cz*

Summary

We present approximate formulae for the plane-wave, displacement reflection/transmission (R/T) coefficients for interfaces of arbitrary contrast, separating two homogeneous, weakly anisotropic media. In deriving them, we use first-order quantities, with which we work when using first-order ray tracing (FORT) for inhomogeneous anisotropic media. Specifically, the phase velocities, slowness and polarization vectors used are of the first-order with respect to the deviations of anisotropy from isotropy. The derived R/T coefficients transform an incident P wave into a reflected/transmitted P or coupled S wave. Coefficients can be computed for any incidence angle between 0^0 and 90^0, and for any azimuth. In this paper, we test the accuracy of the derived R/T coefficients of unconverted plane P waves. We show that, except for critical regions, first-order coefficients approximate the exact coefficients with acceptable accuracy.

Keywords: Body waves; Seismic anisotropy; Wave propagation.

1 Introduction

In our previous papers, we studied the first-order ray tracing and dynamic ray tracing (FORT and FODRT) of seismic body P and coupled S waves propagating in *smoothly varying*, weakly anisotropic media without interfaces (Pšenčík & Farra, 2005, 2007; Farra & Pšenčík, 2008, 2010). To derive the FORT and FODRT equations, we used the perturbation theory, in which deviations of anisotropy from isotropy were considered to be of the first-order. In this paper, we concentrate on computing approximate, first-order reflection/transmission (R/T) coefficients in such media. As in the exact problem of reflection/transmission, the incident and generated waves satisfy boundary conditions corresponding to the given configuration. In case of two elastic, weakly anisotropic solids in welded contact, they are continuity of displacement and traction. The quantities appearing in the boundary conditions are first-order phase velocities, slowness and polarization vectors, with which we work in the FORT and FODRT.

Seismic Waves in Complex 3-D Structures, Report 20, Charles University, Faculty of Mathematics and Physics, Department of Geophysics, Praha 2010, pp.77-102

The study of the R/T problem in anisotropic media has a rather long history. The problem of reflection/transmission of plane waves at a plane interface between two homogeneous anisotropic halfspaces was studied, for example, by Fedorov (1968), Musgrave (1970), Daley & Hron (1977), Graebner (1992), Chapman (1994, 2004). For more references see Červený (2001). Gajewski & Pšenčík (1987) used the plane-wave R/T coefficients in the ray-theory computations of seismic wavefields in 3D laterally varying layered anisotropic media. Considerable attention has been paid to various simplifications of R/T coefficients based, for example, on the assumption of a weak-contrast interface, with anisotropy of the surrounding media of arbitrary strength (e.g., Ursin & Haugen, 1996; Klimeš, 2003) or on the assumption of a weak-contrast interface and weak anisotropy of the surrounding media (e.g., Rueger, 1997, 2002; Vavryčuk & Pšenčík, 1998; Zillmer et al., 1998; Vavryčuk, 1999, Jílek, 2002).

In this paper, we make no weak-contrast interface assumption. We only assume that the media on both sides of the interface are weakly, but generally anisotropic. The assumption of weak anisotropy implies that the S waves involved in the reflection/transmission are coupled. For this reason, the formulation of the reflection/transmission problem resembles closely the formulation for isotropic media. In this paper, we concentrate on incident P waves only. An incident P wave can generate two possible types of waves, P or coupled S waves. The slowness vectors of generated waves are sought by solving numerically the corresponding first-order eikonal equation, separately for each generated wave. The corresponding R/T coefficient is determined by numerically solving a system of six inhomogeneous, linear, algebraic equations. For media with anisotropy of higher symmetry, with specific orientation of symmetry elements with respect to the interface, it might be possible to find explicit expressions for the R/T coefficients (see, e.g., Daley & Hron, 1977; Graebner, 1992). Here, however, we consider the case of general anisotropy.

In Sec.2, we present first-order formulae for the displacement vector $\mathbf{u}$ and traction $\mathbf{T}$ of a P or a coupled S wave. Besides first-order slowness vectors, special attention is paid to the first-order formulae specifying the polarization vector (P waves) or the polarization plane (coupled S waves). These formulae are then used in the boundary conditions in Sec.3. In Sec.3.1, the formulae for and procedure of determining the first-order slowness vectors of generated waves are described. In Sec.3.2, the set of six inhomogeneous linear algebraic equations, from which the first-order R/T coefficients can be determined, see Sec.4, is specified. In Sec.5, the accuracy of the derived formulae for the case of unconverted P waves is studied. Together with the reflection and transmission coefficients, R_{PP} and T_{PP}, the accuracy of the generated first-order slowness and polarization vectors is tested on two models of an isotropic halfspace over an HTI halfspace. The main results are summarized in Sec.6.

The lower-case indices $i, j, k, l, ...$ take the values of 1,2,3, the upper-case indices $I, J, K, L, ...$ take the values of 1,2. The Einstein summation convention over repeated indices is used. The upper index $[\mathcal{M}]$ is used to denote quantities related to the coupled S wave. In order to distinguish quantities related to reflected and transmitted waves, we use superscripts R and T, respectively. Quantities related to the incident wave have no superscript. Sometimes, when we discuss properties of all generated waves, we use the superscript G.

2 First-order expressions for displacement and traction

The boundary conditions, which must be satisfied at an interface, involve displacement vectors $\mathbf{u}$ and tractions $\mathbf{T}$ of the incident and generated waves. We, therefore, specify the first-order approximations of these quantities first.

2.1 Displacement vector

The first-order approximation of the displacement vector $\mathbf{u}$ of an incident or generated harmonic plane wave can be expressed as:

$$\mathbf{u}(\mathbf{x},t) = \mathbf{U}\exp[-\mathrm{i}\omega(t-\mathbf{p}\cdot\mathbf{x})] \ . \tag{1}$$

Here i is the imaginary unit, ω is the circular frequency, $\mathbf{p}$ is the first-order slowness vector and $\mathbf{U}$ is the first-order vectorial amplitude factor.

The first-order slowness vector can be expressed as $\mathbf{p} = \mathbf{n}/c(\mathbf{n})$. Here $\mathbf{n}$ is a unit vector perpendicular to the wavefront of the relevant wave and $c = c(\mathbf{n})$ is its first-order phase velocity. It can be determined from the corresponding first-order eigenvalue of the Christoffel matrix, see below.

The first-order vectorial amplitude factor $\mathbf{U}$ of a plane P wave propagating in a homogeneous, weakly anisotropic medium can be expressed in the following way:

$$\mathbf{U} = \mathcal{C}\mathbf{f}^{[3]} \ . \tag{2}$$

The term $\mathcal{C}$ is the first-order scalar P-wave amplitude factor. The first-order P-wave polarization vector $\mathbf{f}^{[3]}$ is a function of the first-order P-wave slowness vector $\mathbf{p}^{[3]} = \mathbf{n}/c^{[3]}$. Here, $c^{[3]} = c^{[3]}(\mathbf{n})$ is the first-order P-wave phase velocity. Polarization vector $\mathbf{f}^{[3]}$ is given by the expression (Pšenčík & Farra, 2007):

$$\mathbf{f}^{[3]}(\mathbf{p}^{[3]}) = \frac{(c^{[3]})^2(\mathbf{n})}{V_P^2 - V_S^2}[B_{13}(\mathbf{p}^{[3]})\mathbf{e}^{[1]}(\mathbf{p}^{[3]}) + B_{23}(\mathbf{p}^{[3]})\mathbf{e}^{[2]}(\mathbf{p}^{[3]})] + \mathbf{e}^{[3]}(\mathbf{p}^{[3]}) \ . \tag{3}$$

The first-order vectorial amplitude factor $\mathbf{U}$ of a coupled S wave propagating in a homogeneous weakly anisotropic medium can be expressed in the following way (Farra & Pšenčík, 2010):

$$\mathbf{U} = \mathcal{A}\mathbf{f}^{[1]} + \mathcal{B}\mathbf{f}^{[2]} \ . \tag{4}$$

Terms $\mathcal{A}$ and $\mathcal{B}$ are first-order scalar S-wave amplitude factors. Vectors $\mathbf{f}^{[K]} = \mathbf{f}^{[K]}(\mathbf{p}^{[\mathcal{M}]})$ are two mutually perpendicular vectors, to which amplitude factors $\mathcal{A}$ and $\mathcal{B}$ are related. Vectors $\mathbf{f}^{[K]}$ are situated in the plane, which we call the first-order S-wave polarization plane. It is perpendicular to vector $\mathbf{f}^{[3]} = \mathbf{f}^{[3]}(\mathbf{p}^{[\mathcal{M}]})$, where $\mathbf{p}^{[\mathcal{M}]}$ is the first-order slowness vector corresponding to the coupled S wave, $\mathbf{p}^{[\mathcal{M}]} = \mathbf{n}/c^{[\mathcal{M}]}$. Symbol $c^{[\mathcal{M}]} = c^{[\mathcal{M}]}(\mathbf{n})$ denotes the first-order common S-wave phase velocity. Vectors $\mathbf{f}^{[K]}$ are given by the following expressions:

$$\mathbf{f}^{[K]}(\mathbf{p}^{[\mathcal{M}]}) = \mathbf{e}^{[K]}(\mathbf{p}^{[\mathcal{M}]}) - \frac{(c^{[\mathcal{M}]})^2(\mathbf{n})}{V_P^2 - V_S^2}B_{K3}(\mathbf{p}^{[\mathcal{M}]})\mathbf{e}^{[3]}(\mathbf{p}^{[\mathcal{M}]}) \ . \tag{5}$$

Note that vectors $\mathbf{f}^{[i]}$ are generally non-unit and are different for $\mathbf{p}^{[3]}$ and $\mathbf{p}^{[\mathcal{M}]}$.

Symbols B_{13} and B_{23} in eqs (3) and (5) are elements of symmetric matrix $\mathbf{B}(\mathbf{p})$ ($\mathbf{p} = \mathbf{p}^{[3]}$ for P waves and $\mathbf{p} = \mathbf{p}^{[\mathcal{M}]}$ for coupled S waves) with elements:

$$B_{jl}(\mathbf{p}) = \Gamma_{ik}(\mathbf{p}) e_i^{[j]} e_k^{[l]} \ . \tag{6}$$

Terms $\Gamma_{ik}(\mathbf{p})$ are elements of the generalized Christoffel matrix $\mathbf{\Gamma}(\mathbf{p})$:

$$\Gamma_{ik}(\mathbf{p}) = a_{ijkl} p_j p_l \ , \tag{7}$$

where a_{ijkl} are density-normalized elastic moduli. Symbols $e_i^{[j]}$ in eqs (3), (5) and (6) denote the components of three mutually perpendicular unit vectors $\mathbf{e}^{[j]}$. Vector $\mathbf{e}^{[3]}$ has been chosen so that $\mathbf{e}^{[3]} = \mathbf{n}$. Here $\mathbf{n}$ is a unit vector perpendicular to the wavefront, specifying the direction of the first-order slowness vector $\mathbf{p}$ (with components p_i) of the corresponding wave. The remaining two mutually perpendicular unit vectors $\mathbf{e}^{[1]}$ and $\mathbf{e}^{[2]}$ can be chosen arbitrarily in the plane perpendicular to vector $\mathbf{e}^{[3]} = \mathbf{n}$.

Slowness vector $\mathbf{p}$ must satisfy the corresponding first-order eikonal equation

$$G(\mathbf{p}) = 1 \ . \tag{8}$$

Symbol G represents either the first-order approximation of the eigenvalue $G^{[3]}$ of the Christoffel matrix (7), corresponding to the P wave, or an average of the first-order eigenvalues $G^{[1]}$ and $G^{[2]}$ of the Christoffel matrix (7), corresponding to S waves. The explicit form of the first-order eikonal equations for P and coupled S waves can be found in Pšenčík & Farra (2005) and Farra & Pšenčík (2008). The first-order eigenvalues G are closely related to the phase velocities of the corresponding waves

$$(c^{[\mathcal{M}]})^2(\mathbf{n}) = \frac{1}{2}[G^{[1]}(\mathbf{n}) + G^{[2]}(\mathbf{n})] \ , \qquad (c^{[3]})^2(\mathbf{n}) = G^{[3]}(\mathbf{n}) \ . \tag{9}$$

Symbols V_P and V_S in eqs(3) and (5) denote the P- and S-wave velocities corresponding to the reference isotropic medium closely approximating the studied weakly anisotropic medium at the point of incidence. Farra & Pšenčík (2010) showed that, for coupled S waves, the reference velocities must be chosen in the following way:

$$V_S^2 = (c^{[\mathcal{M}]})^2 \ , \quad V_P^2 = (c^{[\mathcal{M}]})^2 B_{33}(\mathbf{p}^{[\mathcal{M}]}) \ . \tag{10}$$

Similarly, we can choose for P waves:

$$V_P^2 = (c^{[3]})^2 \ , \quad V_S^2 = \frac{1}{2}(c^{[3]})^2 [B_{11}(\mathbf{p}^{[3]}) + B_{22}(\mathbf{p}^{[3]})] \ . \tag{11}$$

We can then modify eq.(3) to read:

$$\mathbf{f}^{[3]}(\mathbf{p}^{[3]}) = \frac{B_{13}(\mathbf{p}^{[3]})\mathbf{e}^{[1]}(\mathbf{p}^{[3]}) + B_{23}(\mathbf{p}^{[3]})\mathbf{e}^{[2]}(\mathbf{p}^{[3]})}{1 - \frac{1}{2}[B_{11}(\mathbf{p}^{[3]}) + B_{22}(\mathbf{p}^{[3]})]} + \mathbf{e}^{[3]}(\mathbf{p}^{[3]}) \tag{12}$$

and eq.(5) to read:

$$\mathbf{f}^{[K]}(\mathbf{p}^{[\mathcal{M}]}) = \mathbf{e}^{[K]}(\mathbf{p}^{[\mathcal{M}]}) + \frac{B_{K3}(\mathbf{p}^{[\mathcal{M}]})}{1 - B_{33}(\mathbf{p}^{[\mathcal{M}]})} \mathbf{e}^{[3]}(\mathbf{p}^{[\mathcal{M}]}) \ . \tag{13}$$

2.2 Traction

The components of traction $\mathbf{T}$ acting at an interface with unit normal $\mathbf{N}$ are given by the expression:

$$T_i(\mathbf{x},t) = \tau_{ij}(\mathbf{x},t)N_j = \rho(\mathbf{x})a_{ijkl}(\mathbf{x})N_j u_{k,l}(\mathbf{x},t) \ . \tag{14}$$

See, for example, Gajewski and Pšenčík (1987), Červený (2001). Inserting the expression (1) for the displacement vector into eq.(14) leads to

$$T_i = \mathrm{i}\omega\rho a_{ijkl}N_j U_k p_l \ \exp[-\mathrm{i}\omega(t - \mathbf{p}\cdot\mathbf{x})] \ . \tag{15}$$

The symbols U_k and p_k in eq.(15) represent the components of the first-order vectorial amplitude factors (2) or (4) and of the first-order slowness vectors, respectively.

3 Boundary conditions

Let us consider two homogeneous weakly anisotropic halfspaces in welded contact, separated by plane interface Σ with unit normal $\mathbf{N}$ pointing into the medium, in which the incident plane wave propagates. The medium, in which the incident wave propagates, is specified by density $\rho^{(1)}$ and the density-normalized elastic moduli $a^{(1)}_{ijkl}$. The medium on the other side of the interface is specified by $\rho^{(2)}$ and $a^{(2)}_{ijkl}$. An incident wave generates P and coupled S waves in weakly anisotropic halfspaces on both sides of the interface. The incident and generated waves satisfy the boundary conditions, which in case of an interface separating two solid media, consist in the requirements of continuity of displacement $\mathbf{u}$ and traction $\mathbf{T}$ across the interface.

The boundary conditions lead to two sets of equations. The first set, resulting from the continuity of the traveltime of all involved waves across the interface, represents equations for determining the slowness vectors of generated waves. The second set, resulting from the boundary conditions themselves, represents equations for determining the scalar amplitude factors of generated waves. In the following, we deal successively with both sets of equations.

3.1 Transformation of slowness vectors across an interface

The continuity of traveltime along the interface Σ implies the continuity of the traveltime derivatives taken along the interface. This can be expressed in the following way:

$$\mathbf{p}^G - (\mathbf{p}^G\cdot\mathbf{N})\mathbf{N} = \mathbf{p} - (\mathbf{p}\cdot\mathbf{N})\mathbf{N} \ . \tag{16}$$

Here, $\mathbf{p}$ and $\mathbf{p^G}$ are first-order slowness vectors of the incident and generated (G) waves, $\mathbf{N}$ is the unit normal to interface Σ. Eq.(16) represents the Snell law for anisotropic media. From equation (16) we can determine the components of the slowness vectors of the generated waves, tangential to the interface. It remains to determine their components along the normal $\mathbf{N}$ to the interface. We can express the slowness vectors of generated waves as

$$\mathbf{p}^G = \mathbf{b} + \xi^G\mathbf{N} = \mathbf{p} - (\mathbf{p}\cdot\mathbf{N})\mathbf{N} + \xi^G\mathbf{N} \ . \tag{17}$$

In eq.(17), ξ^G represents the scalar component of $\mathbf{p}^G$ to $\mathbf{N}$, and $\mathbf{b}$ represents the vectorial component of $\mathbf{p}^G$, tangential to Σ. Components ξ^G are the sought parameters. They can be found from the first-order eikonal equations satisfied by the waves generated on corresponding sides of the interface

$$G(\mathbf{b} + \xi^G \mathbf{N}) = 1 \ . \tag{18}$$

Eikonal equation (18) can be rewritten into the form of a polynomial equation of the fourth degree in ξ^G. It has four roots, two of which are non-physical. They can be identified as two conjugate roots, whose imaginary parts are larger than the imaginary parts of the remaining two roots. Of the remaining two roots, we accept the one, whose first-order ray-velocity vector $\mathbf{v}^G$ ($v_i^G = \frac{1}{2}\partial G/\partial p_i$, where $G = G^{[3]}$ for P waves, or $G = \frac{1}{2}(G^{[1]} + G^{[2]})$ for coupled S waves) points into the medium, in which the generated wave should propagate (in case of real roots) or which satisfies the radiation condition (in case of complex conjugate roots). Explicitly this means that $N_i v_i^G \geq 0$ for reflected and $N_i v_i^G \leq 0$ for transmitted waves in case of real roots, and $\mathrm{Im}\xi^G \geq 0$ for reflected and $\mathrm{Im}\xi^G \leq 0$ for transmitted waves in case of complex conjugate roots. The waves corresponding to the real roots of the polynomial equation are regular waves while those related to the complex roots are evanescent waves.

The selection of roots described above can be used in employing a polynomial equation solver, which provides all four roots. We can, however, also use alternative procedures. In weakly anisotropic media, it is reasonable to assume that the sought root of eq.(18) is close to the root $\xi^{G(0)}$ of a similar equation corresponding to a reference isotropic medium. We can thus use the root from the reference isotropic case as an initial guess of the sought root. Jech & Pšenčík (1989, Sec.4.3) proposed a one-step procedure based on the first-order correction of such an initial guess $\xi^{G(0)}$. Recently, Vanelle & Gajewski (2009) made the procedure iterative, updating successively the reference isotropic medium. The procedure proposed and used by Dehghan, Farra & Nicolétis (2007) seems to be more efficient. They also use $\xi^{G(0)}$, determined for a reference isotropic medium, as the initial value in the iterative search for the solution of eq.(18). Rather than updating the reference medium, they use the Newton-Raphson iterative method to update the root itself. The iterative formula, derived from the expansion of the eigenvalue G in eq.(18) with respect to ξ^G, reads:

$$\mathbf{p}^{G\{j\}} = \mathbf{b} + \xi^{G\{j\}} \mathbf{N} \ , \tag{19}$$

where j is the iteration number and

$$\xi^{G\{j\}} = \xi^{G\{j-1\}} - \frac{G(\mathbf{p}^{G\{j-1\}}) - 1}{N_k \partial G/\partial p_k(\mathbf{p}^{G\{j-1\}})} \ . \tag{20}$$

The explicit expressions for G and $\partial G/\partial p_k$ for P waves in media of arbitrary anisotropy and for coupled S waves in media of orthorhombic and TI symmetries can be found in Pšenčík & Farra (2007) and Farra & Pšenčík (2008), respectively. The expression for $\partial G/\partial p_k$ for coupled S waves in media of arbitrary anisotropy can be simply determined by differentiating eq.(19) of Farra & Pšenčík (2008) with respect to p_k.

The use of eqs(19) and (20) avoids the necessity of seeking the best-fitting reference medium (Vanelle & Gajewski, 2009). The procedure described above can be used even for stronger anisotropy and arbitrary incidence angles, including large ones. It can also be used to seek the roots of eq.(18) for evanescent waves, i.e. to seek complex-valued roots.

3.2 Transformation of amplitudes across an interface

The continuity of traveltime along interface Σ leads to the equality of the exponential factors of displacement vectors of incident and generated waves. Taking this into account, we can express the boundary conditions as follows

$$\mathcal{A}^R f_i^{[1]R} + \mathcal{B}^R f_i^{[2]R} + \mathcal{C}^R f_i^{[3]R} - \mathcal{A}^T f_i^{[1]T} - \mathcal{B}^T f_i^{[2]T} - \mathcal{C}^T f_i^{[3]T} = -U_i \ ,$$

$$\mathcal{A}^R X_i^{[1]R} + \mathcal{B}^R X_i^{[2]R} + \mathcal{C}^R X_i^{[3]R} - \mathcal{A}^T X_i^{[1]T} - \mathcal{B}^T X_i^{[2]T} - \mathcal{C}^T X_i^{[3]T} = -X_i \ , \tag{21}$$

where

$$X_i = \rho^{(1)} a_{ijkl}^{(1)} N_j U_k p_l \ ,$$

$$X_i^{[3]R} = \rho^{(1)} a_{ijkl}^{(1)} N_j f_k^{[3]R} p_l^{[3]R} \ , \quad X_i^{[3]T} = \rho^{(2)} a_{ijkl}^{(2)} N_j f_k^{[3]T} p_l^{[3]T} \ ,$$

$$X_i^{[N]R} = \rho^{(1)} a_{ijkl}^{(1)} N_j f_k^{[N]R} p_l^{[\mathcal{M}]R} \ , \quad X_i^{[N]T} = \rho^{(2)} a_{ijkl}^{(2)} N_j f_k^{[N]T} p_l^{[\mathcal{M}]T} \ . \tag{22}$$

The symbols X_i in eqs (21) and (22) correspond to the incident wave, symbols $X_i^{[3]G}$ to generated P waves and $X_i^{[N]G}$, $N = 1, 2$, to generated coupled S waves. The slowness vectors of generated waves are determined by the procedure described in the preceding section. Vectors $\mathbf{f}^{[i]G}$ can be determined from eqs (3) or (5) or, alternatively, from eqs (12) or (13).

4 R/T coefficients for the incident P wave

For the incident P wave, the quantities U_i and X_i on the right-hand side of eq.(21) follow from (2) and from the first equation in (22), in which U_k again follows from (2) and p_l are the components of the P-wave first-order slowness vector $\mathbf{p}^{[3]}$.

Eqs (21) represent a set of six inhomogeneous linear algebraic equations for six unknowns $\mathcal{A}^R$, $\mathcal{B}^R$, $\mathcal{C}^R$, $\mathcal{A}^T$, $\mathcal{B}^T$ and $\mathcal{C}^T$, the first-order scalar amplitude factors of four waves generated by incidence of the wave with the first-order vectorial amplitude factor $\mathbf{U}$. If we wish to compute the standard displacement R/T coefficients, we have to modify eqs (21) and (22). It is necessary to normalize the vectors $\mathbf{f}^{[i]}$ and $\mathbf{f}^{[i]G}$ in (21) and (22) to unit vectors, and to replace them by their normalized counterparts $\bar{\mathbf{f}}^{[i]}$ and $\bar{\mathbf{f}}^{[i]G}$. Normalized vectors $\bar{\mathbf{f}}^{[I]G}$ can be chosen arbitrarily in the plane perpendicular to vector $\mathbf{f}^{[3]G}$. It is now possible to introduce first-order R/T coefficients as $R_{PP} = \nu^{[3]R}\mathcal{C}^R/\mathcal{C}$, $T_{PP} = \nu^{[3]T}\mathcal{C}^T/\mathcal{C}$, $R_{PS[1]} = \nu^{[1]R}\mathcal{A}^R/\mathcal{C}$, $R_{PS[2]} = \nu^{[2]R}\mathcal{B}^R/\mathcal{C}$, $T_{PS[1]} = \nu^{[1]T}\mathcal{A}^T/\mathcal{C}$ and $T_{PS[2]} = \nu^{[2]T}\mathcal{B}^T/\mathcal{C}$, where $\nu^{[i]R} = |\mathbf{f}^{[i]R}|/|\mathbf{f}^{[i]}|$ and $\nu^{[i]T} = |\mathbf{f}^{[i]T}|/|\mathbf{f}^{[i]}|$. Indices $S[1]$ and $S[2]$ indicate that the corresponding coefficients are related to vectors $\bar{\mathbf{f}}^{[1]G}$ or $\bar{\mathbf{f}}^{[2]G}$, respectively. Eqs(21) and (22) can now be expressed in the following form:

$$\begin{aligned} R_{PS[1]}\bar{f}_i^{[1]R} + R_{PS[2]}\bar{f}_i^{[2]R} + R_{PP}\bar{f}_i^{[3]R} - T_{PS[1]}\bar{f}_i^{[1]T} - T_{PS[2]}\bar{f}_i^{[2]T} - T_{PP}\bar{f}_i^{[3]T} &= -\bar{f}_i^{[3]} \ , \\ R_{PS[1]}\bar{X}_i^{[1]R} + R_{PS[2]}\bar{X}_i^{[2]R} + R_{PP}\bar{X}_i^{[3]R} - T_{PS[1]}\bar{X}_i^{[1]T} - T_{PS[2]}\bar{X}_i^{[2]T} - T_{PP}\bar{X}_i^{[3]T} & \\ = -\rho^{(1)} a_{ijkl}^{(1)} N_j \bar{f}_k^{[3]} p_l \ , & \end{aligned} \tag{23}$$

where

$$\bar{X}_i^{[3]R} = \rho^{(1)} a_{ijkl}^{(1)} N_j \bar{f}_k^{[3]R} p_l^{[3]R} \ , \quad \bar{X}_i^{[3]T} = \rho^{(2)} a_{ijkl}^{(2)} N_j \bar{f}_k^{[3]T} p_l^{[3]T} \ ,$$
$$\bar{X}_i^{[N]R} = \rho^{(1)} a_{ijkl}^{(1)} N_j \bar{f}_k^{[N]R} p_l^{[\mathcal{M}]R} \ , \quad \bar{X}_i^{[N]T} = \rho^{(2)} a_{ijkl}^{(2)} N_j \bar{f}_k^{[N]T} p_l^{[\mathcal{M}]T} \ . \tag{24}$$

5 Examples

In this section, the system of eqs (23) with (24) is used to calculate the first-order R_{PP} and T_{PP} coefficients. Since we are interested in unconverted P waves, the choice of vectors $\bar{\mathbf{f}}^{[I]}$ in the plane perpendicular to $\mathbf{f}^{[3]}$ can be arbitrary. We determine them from eq.(13), in which vector $\mathbf{e}^{[2]}$ is chosen horizontal and all three vectors $\mathbf{e}^{[i]}$ form an orthonormal right-handed vectorial basis.

For tests of accuracy of the first-order coefficients and related quantities, we use the two models used by Pšenčík & Vavryčuk (1998). In both models, we consider an isotropic halfspace, in which an incident wave propagates, over the HTI halfspace. The lower HTI halfspace is the same in both models. The models differ only in the upper isotropic halfspace. In the first model, Model A, the P- and S-wave velocities and density of the upper halfspace are $\alpha = 4.0$ km/s, $\beta = 2.31$ km/s and $\rho = 2.65$ g/cm^3, respectively. In the second model, Model B, these parameters are $\alpha = 3.0$ km/s, $\beta = 1.73$ km/s and $\rho = 2.2$ g/cm^3. The matrix of density-normalized elastic moduli (in km^2/s^2) specifying the HTI medium of the lower halfspace reads:

$$\begin{pmatrix} 9.43 & 3.14 & 3.14 & 0.00 & 0.00 & 0.00 \\ & 15.27 & 4.60 & 0.00 & 0.00 & 0.00 \\ & & 15.27 & 0.00 & 0.00 & 0.00 \\ & & & 5.33 & 0.00 & 0.00 \\ & & & & 4.25 & 0.00 \\ & & & & & 4.25 \end{pmatrix} \ . \tag{25}$$

The density of the HTI medium is $\rho = 2.6$ g/cm^3. We can see that the axis of symmetry is oriented along the x-axis of the Cartesian coordinate system. The vertical sections of the phase-velocity surfaces containing the horizontal axis of symmetry are shown in Figure 1. The P-wave velocity section is shown in the bottom plot, the S-wave velocity sections are shown in the top plot.

We can see that in Model A, the P- and S-wave velocities in the upper (isotropic) halfspace exceed the P- and S-wave velocities in the lower halfspace. Except for vertical plane perpendicular to the axis of symmetry, the velocity contrast (ratio of the absolute value of the difference of velocities on both sides of the interface and of their average) varies with the incidence angle. For P waves in the vertical plane containing the axis of symmetry, the velocity contrast increases from about 2% for vertical incidence (0^0) to about 26% for nearly tangential incidence (90^0). For the S1 wave (faster, with SH-wave polarization) in the same vertical plane, the contrast increases from about 0.05% to about 11%. For the S2 wave (slower), the contrast slightly varies around 11%. In Model B, the P- and S-wave velocities in the upper halfspace are lower than in the lower halfspace. The

contrast is generally higher than in Model A. Its variation in the vertical plane containing axis of symmetry is opposite to that for Model A. For the P wave, the contrast decreases from about 26% for normal incidence to about 2% for nearly tangential incidence. For the S1 wave, the contrast decreases from about 29% to 17%. For the S2 wave, the contrast varies slightly around 17%. As to the anisotropy of the HTI halfspace, it is about 24% for the P wave and around 11% for the S1 wave.

Coefficients R_{PP} and T_{PP} obtained by solving the system of equations (23) may be complex valued. Therefore, we present them in terms of their moduli and phases:

$$R_{PP} = |R| \exp(\mathrm{i}\varphi_R) \ , \qquad T_{PP} = |T| \exp(\mathrm{i}\varphi_T) \ . \tag{26}$$

The presented figures have the forms of maps, in which the quantities are shown as functions of the angle of incidence θ (horizontal axis) and of azimuth Φ (vertical axis). Both angles are specified in degrees. Azimuth $\Phi = 0^0$ corresponds to the direction along the axis of symmetry, $\Phi = 90^0$ to the direction perpendicular to the axis of symmetry. The incidence angle $\theta = 0^0$ corresponds to normal incidence.

For a better understanding of the behaviour of the approximate coefficients, we first show the maps of deviations of the first-order quantities as slowness or polarization vectors, or polarization planes of waves generated in the lower anisotropic halfspace from their exact counterparts. These deviations are expressed as angles (in degrees) made by the approximate and exact vectors. We then show maps of the exact moduli and phases of the R_{PP} and T_{PP} coefficients followed by maps of differences of the moduli and phases of the first-order R/T coefficients from the exact ones.

Figure 2 shows the maps of angular deviations of the approximate and exact slowness vectors of the transmitted P (top), S1 (middle) and S2 (bottom) waves for Model A. The S-wave plots show the deviations of the first-order slowness vectors of coupled S wave from the exact slowness vectors of S1 and S2 waves. Similar maps for the reflected P and S waves are not shown because the reflected waves propagate in the isotropic halfspace, in which the approximate slowness vectors coincide with the exact vectors (thus their differences are zero for each incidence angle and azimuth).

We can see that the approximate slowness vectors of the P wave do not deviate from the exact vectors by more than 1^0. The deviations increase with increasing angle of incidence, the maximum deviations occurring for azimuths around 50^0. Deviations are zero and close to zero for azimuth 90^0 and azimuths close to it. The vertical plane with azimuth 90^0 is perpendicular to the axis of symmetry and thus coincides with the "isotropy plane", in which directions of approximate slowness vectors coincide with exact slowness vectors. The situation is different in case of S waves (middle and bottom plots). The deviations also increase with increasing angle of incidence, being largest for azimuths around 90^0. They are slightly larger than in the case of the P wave; they slightly exceed 2^0. For azimuths close to 90^0, we observe non-zero deviations. This is the consequence of studying the deviations of the first-order slowness vectors, corresponding to the coupled S wave, from the exact slowness vectors of separate S1 and S2 waves, as mentioned above.

We have also studied differences in the size of the approximate and exact slowness vectors. We found that the differences do not exceed 1% for P waves and 6% for S waves.

Figure 3 shows the maps of angular deviations of the approximate and exact polariza-

tion of transmitted P (top) and S (bottom) waves for Model A. In the case of P waves, we show the deviations of the first-order polarization vectors (3) from the exact ones. In the case of S waves, we show the deviations of the normal to the first-order S-wave polarization plane, formed by vectors $\mathbf{f}^{[K]}$ in eq.(5), from the normal to the exact S-wave polarization plane, defined by the exact S-wave polarization vectors. For the same reasons as in the case of the deviations of slowness vectors, the maps for reflected P and S waves are not shown. The behaviour of the polarization deviations is similar to the behaviour of the slowness vector deviations. In the case of P waves, the deviations of the polarization vectors are slightly larger, slightly exceeding 1.2^0. The deviations for azimuths close to 90^0 are zero. The deviations of the polarization vectors of S waves resemble deviations of slowness vectors of S waves very closely.

In Figure 4, we can see maps of the modulus of the exact R_{PP} coefficient (top) and of the differences of moduli of the first-order and the exact R_{PP} coefficients (bottom) for Model A. Because of higher velocities in the upper halfspace, there are no critical reflections. For all the azimuths and incidence angles, the phases are π (therefore, we do not show the map of phases), which indicates that the coefficients are negative. The first-order coefficients also have phase π, therefore, the differences in phase are zero everywhere and are not shown. Since the contrast is very weak for small angles of incidence, the modulus of the exact R_{PP} coefficient is rather small for small angles. As expected, modulus $|R_{PP}|$ increases, except for incidence angles close to 20^0 and azimuths between 0 and 40^0, with increasing incidence angle. The slight decrease of coefficients in the above-mentioned region is an effect observable only in anisotropic media. From the bottom plot, we can see that, for small incidence angles, the approximate R_{PP} coefficient is less than the exact one. Only for large azimuths and large incidence angles, are the approximate coefficients slightly larger than the exact ones. For azimuths close to 90^0 (isotropy plane) or small angles of incidence, the approximate R_{PP} coefficient is very accurate. The errors are smaller at least by one order, but for most angles of incidence significantly less than the values of the R_{PP} coefficient. The relative errors of the first-order coefficient in regions, in which the exact coefficient is about 0.1, or larger, do not exceed 3%. In regions, where the exact coefficient is very small, the relative errors are, of course, larger. They may reach 25%.

Figure 5 shows the same as Fig.4, but for the transmission coefficient T_{PP} for Model A. The modulus of the T_{PP} coefficient decreases with increasing incidence angle. Due to the weak-contrast interface for small angles of incidence, the values of the T_{PP} coefficient are quite large for these angles. The phase is zero for any angle of incidence and azimuth. From the bottom plot, we can see that the approximate T_{PP} coefficient is less than the exact one for all azimuths and angles of incidence. The differences are smaller by at least two orders than the values of the coefficient. The maximum difference is about 0.015. The relative errors are less than 1% for most angles, slightly exceeding 3% for large incidence angles.

In the following figures, we show plots corresponding to Model B. As mentioned above, in this case the velocities in the isotropic halfspace are smaller than in the lower anisotropic halfspace. We can, therefore, observe critical and overcritical incidence of P wave. The effects of critical and overcritical incidence can already be observed in maps of the angular deviations of approximate and exact slowness vectors.

Angular deviations of the first-order and exact slowness vectors of transmitted P (top), S1 (middle) and S2 (bottom) waves are shown in Figure 6. If we compare the top plots of Figs 2 and 6, we can see a similar increase in deviations for increasing angles of incidence up to certain "boundary" values (angles of incidence of about 75^0 for azimuths close to 0^0, which continuously change to angles of incidence of about 50^0 for azimuths close to 90^0). The deviations in the upper plot of Fig.6 grow quickly round these "boundary" values of the angles of incidence. These angles of incidence indicate critical incidence. Since the angular positions of exact and approximate critical angles slightly differ, we can observe a narrow belt (instead of a sharp curve), in which the angular deviations increase over the value of about 1.5^0, the maximum value in the subcritical region. In the overcritical region, the angular differences are zero. This is because we are comparing the real parts of the complex-valued first-order and exact slowness vectors in this region. The real parts are in both cases tangent to the interface and thus their angular difference is zero. As in Fig.2, the differences for the azimuths close to 90^0 are negligible. The slowness vectors of transmitted S waves are not affected by overcritical incidence and, therefore, the behaviour of their deviations is very similar to the behaviour of their counterparts in Model A, shown in the middle and bottom plots of Fig.2. The deviations in Model B attain greater values (up to around 3^0) as a consequence of the lower velocities in the upper halfspace than in the lower.

Similarly as in Model A, the differences in the size of the approximate and exact slowness vectors do not exceed 1% for P waves and 6% for S waves.

In the upper plot of Fig.7, which shows the angular deviations of the first-order and exact P-wave polarization vectors in the lower halfspace of Model B, we can again observe a narrow belt of strongly increased values of deviations, which indicates the region of critical incidence. In the subcritical region, the differences behave in a similar way as in the upper plot of Fig.3, with slightly higher angular deviations of the first-order and exact polarization vectors, which are again the consequence of lower velocities in the upper halfspace. This is also true for any angle of incidence and azimuth for the S-wave polarization differences shown in the bottom plot of Fig.7; compare this plot and the bottom plot of Fig.3.

Fig.8 shows maps of the modulus of the exact R_{PP} coefficient (top) and of the differences of moduli of approximate and exact R_{PP} coefficients (bottom) for Model B. We can see that the behaviour of the modulus of the exact coefficient is dramatically different from the behaviour of $|R_{PP}|$ in Model A (see upper plot of Fig.4). We can clearly see the region of increased density of isolines, which indicates critical incidence. As we have already seen in the upper plots of Figs 6 and 7, it varies from angles of incidence of about 75^0 for azimuths around 0^0 to angles of incidence of about 50^0 for azimuths close to 90^0. The variation of the R_{PP} coefficient in the overcritical region is negligible in comparison with the variation in the subcritical region. An interesting phenomenon can be observed for small azimuths and angles of incidence around 70^0. Along one of the isolines in this region (not shown in the plot), the modulus of the R_{PP} coefficient becomes zero. The angles of incidence along this isoline, which can be seen much better in the bottom plot of Fig.8 (angles of incidence between 53^0 and 71^0 and azimuths between 0^0 and 16^0), represent Brewster angles, for which the reflection coefficient is zero. Except for a slight shift of isolines, the map of the first-order R_{PP} coefficient (not shown) is identical with the upper plot of Fig.8. Therefore, the differences shown in the bottom plot of Fig.8

are generally very small. They only increase significantly in the vicinity of critical incidence and also close to the above-mentioned Brewster angles. The increased density of isolines is the consequence of the slight misposition of the critical and Brewster angles of the approximate and exact coefficients and of their rapid variations in the mentioned regions. Except for these narrow regions, there are no dramatic differences between the approximate and exact coefficients.

For subcritical incidence, the phases, with the exception of the vicinity of the Brewster angles (the isoline between azimuths 53^0 and 71^0 and between the angles of incidence 0^0 and 16^0), are zero. For overcritical incidence, the phases become non-zero and vary as shown (in degrees) in the upper plot of Fig.9. At Brewster angles, the phases switch from zero (outside the above-mentioned isoline) to π (inside). The differences in phases (in degrees again) shown in the bottom plot indicate that, except for the close vicinity of critical incidence and the Brewster angles (again caused by misposition of the isolines for approximate and exact phases), the approximate phases differ only a little from the exact.

Figure 10 shows transmission coefficient T_{PP} for Model B. The modulus of the T_{PP} coefficient (top) increases smoothly with the incidence angle up to critical incidence. It then decreases rapidly to zero for tangential incidence. There are no Brewster angles for the T_{PP} coefficient. Although the region of critical incidence in the plot of the modulus of the T_{PP} coefficient is difficult to identify (it is between the isolines of 1.5), it is clearly visible in the plot of differences of approximate and exact coefficients (bottom). Except for the region of critical incidence, the differences between the first-order and exact coefficients are again very small.

As in the case of the reflection coefficient, the phases of the transmission coefficients are zero for subcritical incidence. They become non-zero for overcritical incidence, see the upper plot in Figure 11, where they are again shown in degrees. Except for the region of critical incidence, the differences between approximate and exact phases are, as in Fig.9, very small.

6 Concluding remarks

A characteristic and important feature of the first-order coefficients presented in this paper is their applicability to all incidence angles and azimuths. For example, the approximate coefficients of Vavryčuk & Pšenčík (1998), Zillmer et al.(1998), Jílek (2002), Rueger (2002), Klimeš (2003) are applicable only to smaller angles of incidence; they are inapplicable for critical and overcritical reflections and/or transmissions. Another advantage of the approximate coefficients presented in this paper is their applicability to models with arbitrary contrast. The coefficients of the above-mentioned references are applicable only to weak-contrast models. It is also important to emphasize that S waves in weakly anisotropic media are considered as one coupled S wave in the described first-order R/T coefficients. This was not the case in previous studies of R/T coefficients. The only limitation of the presented coefficients is their applicability to weakly anisotropic media.

The described tests of the first-order R_{PP} and T_{PP} coefficients and related quantities such as slowness and polarization vectors indicate the high accuracy of the approximate formulae. Exceptions are only in the close vicinities of critical incidence and of the Brewster angles. In applications in the ray theory, the inaccuracies of R/T coefficients in the vicinities of critical incidence are not a problem since the ray theory itself does not work properly in these regions.

Acknowledgements

A substantial part of this work was done during IP's stay at the IPG Paris at the invitation of the IPGP. We are grateful to the Consortium Project "Seismic waves in complex 3-D structures" (SW3D) and Research Project 205/08/0332 of the Grant Agency of the Czech Republic for support.

References

Červený, V., 2001. *Seismic Ray Theory*, Cambridge Univ. Press, Cambridge.

Chapman, C. H., 1994. Reflection/transmission coefficient reciprocities in anisotropic media. *Geophys.J.Int.*, **116**, 498-501.

Chapman, C. H., 2004. *Fundamentals of seismic wave propagation*. Cambridge: Cambridge Univ. Press.

Daley, P.F., & Hron, F., 1977. Reflection and transmission coefficients for transversely isotropic media. *Bull. Seismol. Soc. Am.*, **67**, 661–675.

Dehghan, K., Farra, V. & Nicolétis, L., 2007. Approximate ray tracing for qP-waves in inhomogeneous layered media with weak structural anisotropy. *Geophysics*, **72**, SM47–SM60.

Farra, V. & Pšenčík, I., 2008. First-order ray computations of coupled S waves in inhomogeneous weakly anisotropic media. *Geophys.J.Int.*, **173**, 979-989.

Farra, V. & Pšenčík, I., 2010. Coupled S waves in inhomogeneous weakly anisotropic media using first-order ray tracing. *Geophys.J.Int.*, **180**, 405–417.

Fedorov, F.I., 1968. *Theory of elastic waves in crystals*, Plenum, New York.

Gajewski, D. & Pšenčík, I., 1987. Computation of high-frequency seismic wavefileds in 3-D laterally inhomogeneous anisotropic media. *Geophys.J.R.astr.Soc.*, **91**, 383–411.

Graebner, M., 1992. Plane-wave reflection and transmission coefficients for a transversely isotropic solid. *Geophysics*, **57**, 1512–1519.

Jech, J. & Pšenčík, I., 1989. First-order perturbation method for anisotropic media. *Geophys.J.Int.*, **99**, 369–376.

Jílek, P., 2002. Converted PS-wave reflection coefficients in weakly anisotropic media. *Pure Appl. Geophys.*, **159**, 1527–1562.

Klimeš, L., 2003. Weak-contrast reflection-transmission coefficients in a generally anisotropic background. *Geophysics*, **68**, 2063–2072.

Musgrave, M.P.J., 1970. *Crystal Acoustics*, Holden-Day, San Francisco.

Pšenčík, I. & Farra, V., 2005. First-order ray tracing for qP waves in inhomogeneous weakly anisotropic media. *Geophysics*, **70**, D65–D75.

Pšenčík, I. & Farra, V., 2007. First-order P-wave ray synthetic seismograms in inhomogeneous weakly anisotropic media. *Geophys.J.Int.*, **170**, 1243–1252.

Pšenčík,I. & Vavryčuk,V., 1998. PP wave displacement R/T coefficients in weakly anisotropic media, *PAGEOPH*, **151**, 699–718.

Rueger, A., 1997. P-wave reflection coefficients for transversely isotropic models with vertical and horizontal axis of symmetry. *Geophysics*, **62**, 713-722.

Rueger, A., 2002. *Reflection Coefficients and Azimuthal AVO Analysis in Anisotropic Media*, SEG, Tulsa.

Ursin, B., & Haugen,G.U., 1996. Weak-contrast approximation of the elastic scattering matrix in anisotropic media. *Pure Appl. Geophys.*, **148**, 685-714.

Vanelle, C. & Gajewski, D., 2009. Application of Snell's law in weakly anisotropic media. *Geophysics*, **74**, WB147–WB152.

Vavryčuk, V., 1999. Weak-contrast R/T coefficients in weakly anisotropic elastic media: P-wave incidence. *Geophys. J. Int.*, **138**, 553–562.

Vavryčuk, V., & Pšenčík, I., 1998. PP wave reflection coefficients in weakly anisotropic media, *Geophysics*, **63**, 2129–2141.

Zillmer, M., Gajewski,D., & Kashtan,B. M.. 1998, Anisotropic reflection coefficients for a weak-contrast interface. *Geophys. J. Int.*, **132**, 159-166.

Figure captions

Figure 1: The P-wave (bottom) and S-waves (top) vertical velocity sections containing the axis of symmetry of the HTI medium specified in (25). The velocities vary from the vertical (0^0) to horizontal (90^0) direction of the wave normal.

Figure 2: Maps of the angular deviations (in degrees) of approximate and exact slowness vectors of transmitted P (top), S1 (middle) and S2 (bottom) waves for Model A.

Figure 3: Maps of the angular deviations (in degrees) of approximate and exact polarization vectors of transmitted P (top) and of polarization planes of S (bottom) waves for Model A.

Figure 4: Maps of the moduli of the exact R_{PP} coefficient (top) and of the differences of moduli of the first-order and exact R_{PP} coefficients (bottom) for Model A.

Figure 5: Maps of the moduli of the exact T_{PP} coefficient (top) and of the differences of moduli of the first-order and exact T_{PP} coefficients (bottom) for Model A.

Figure 6: Maps of the angular deviations (in degrees) of approximate and exact slowness vectors of transmitted P (top), S1 (middle) and S2 (bottom) waves for Model B.

Figure 7: Maps of the angular deviations (in degrees) of approximate and exact polarization vectors of transmitted P (top) and of polarization planes of S (bottom) waves for Model B.

Figure 8: Maps of the moduli of the exact R_{PP} coefficient (top) and of the differences of moduli of the first-order and exact R_{PP} coefficients (bottom) for Model B.

Figure 9: Maps of the phase (in degrees) of the exact R_{PP} coefficient (top) and of the differences of phases of the first-order and exact R_{PP} coefficients (bottom) for Model B.

Figure 10: Maps of the moduli of the exact T_{PP} coefficient (top) and of the differences of moduli of the first-order and exact T_{PP} coefficients (bottom) for Model B.

Figure 11: Maps of the phase (in degrees) of the exact T_{PP} coefficient (top) and of the differences of phases of the first-order and exact T_{PP} coefficients (bottom) for Model B.

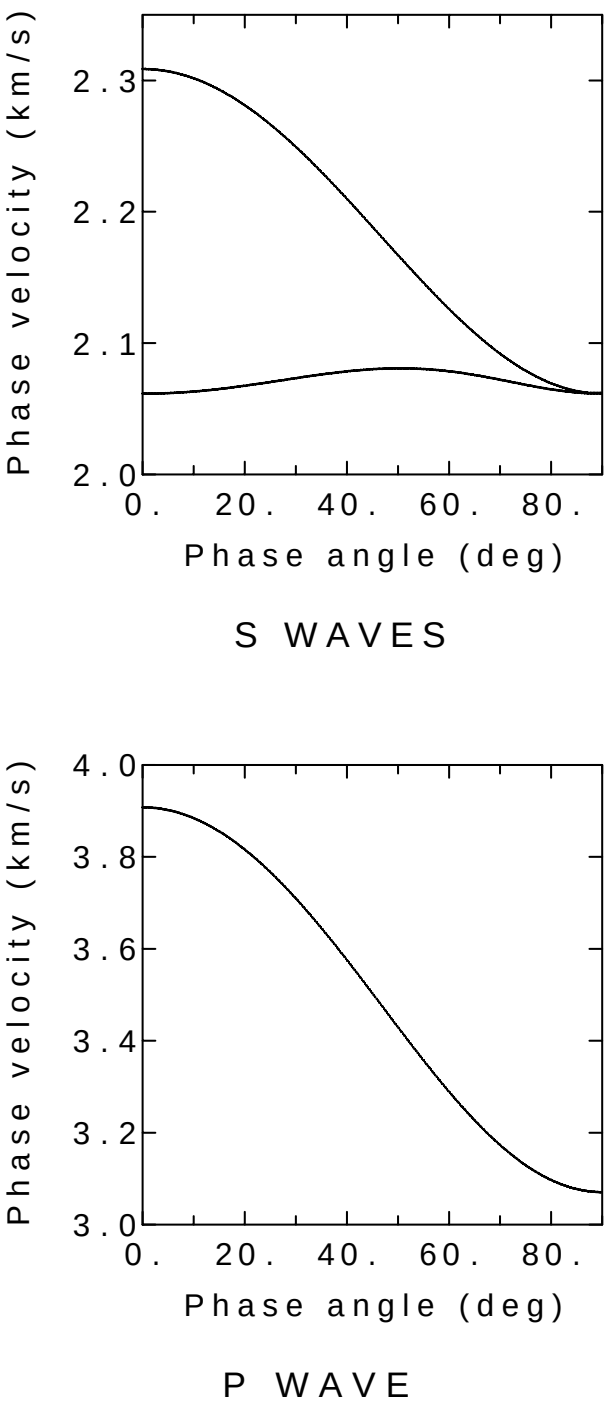

Figure 1: The P-wave (bottom) and S-waves (top) vertical velocity sections containing the axis of symmetry of the HTI medium specified in (25). The velocities vary from the vertical (0^0) to horizontal (90^0) direction of the wave normal.

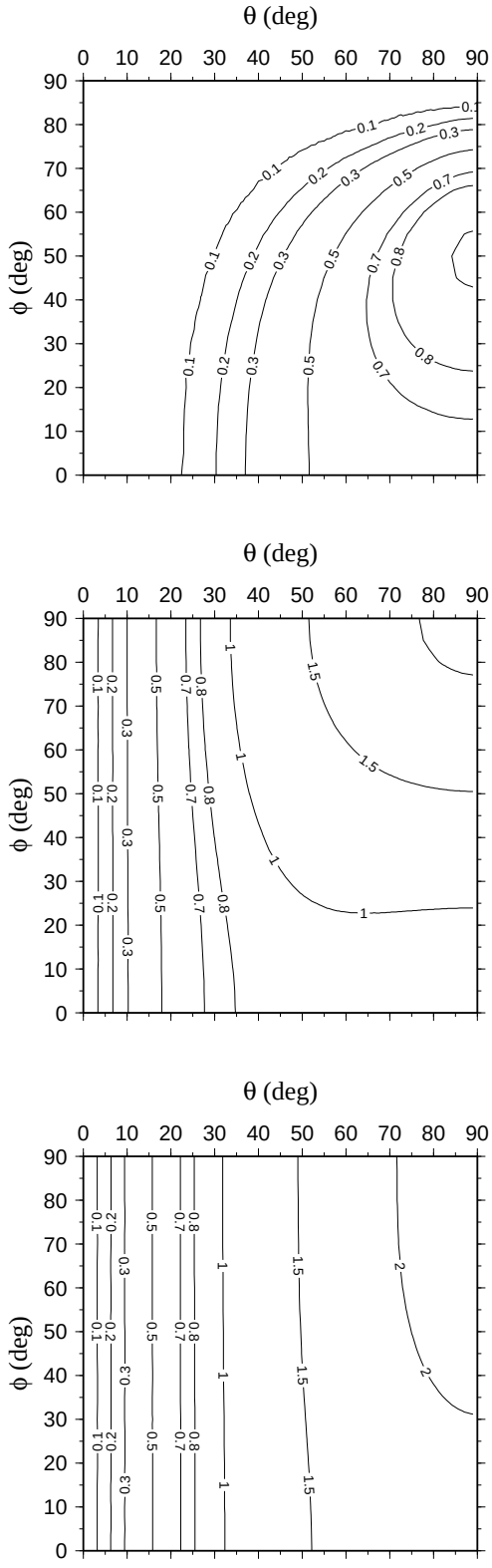

Figure 2: Maps of the angular deviations (in degrees) of approximate and exact slowness vectors of transmitted P (top), S1 (middle) and S2 (bottom) waves for Model A.

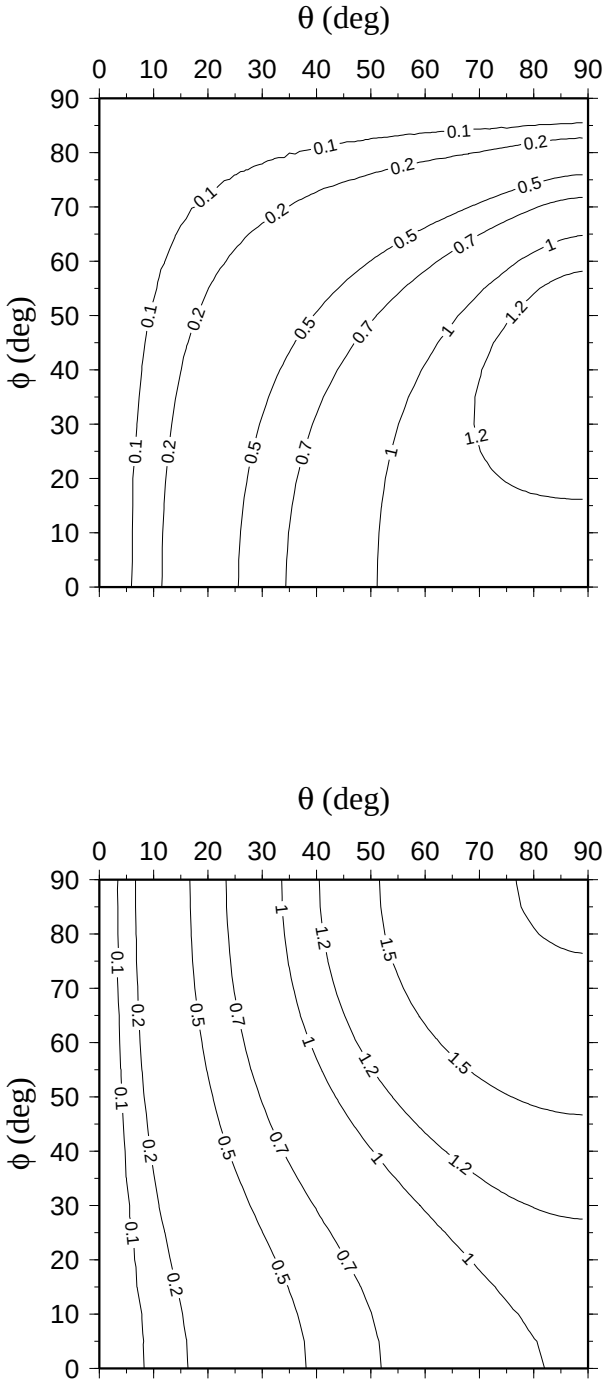

Figure 3: Maps of the angular deviations (in degrees) of approximate and exact polarization vectors of transmitted P (top) and of polarization planes of S (bottom) waves for Model A.

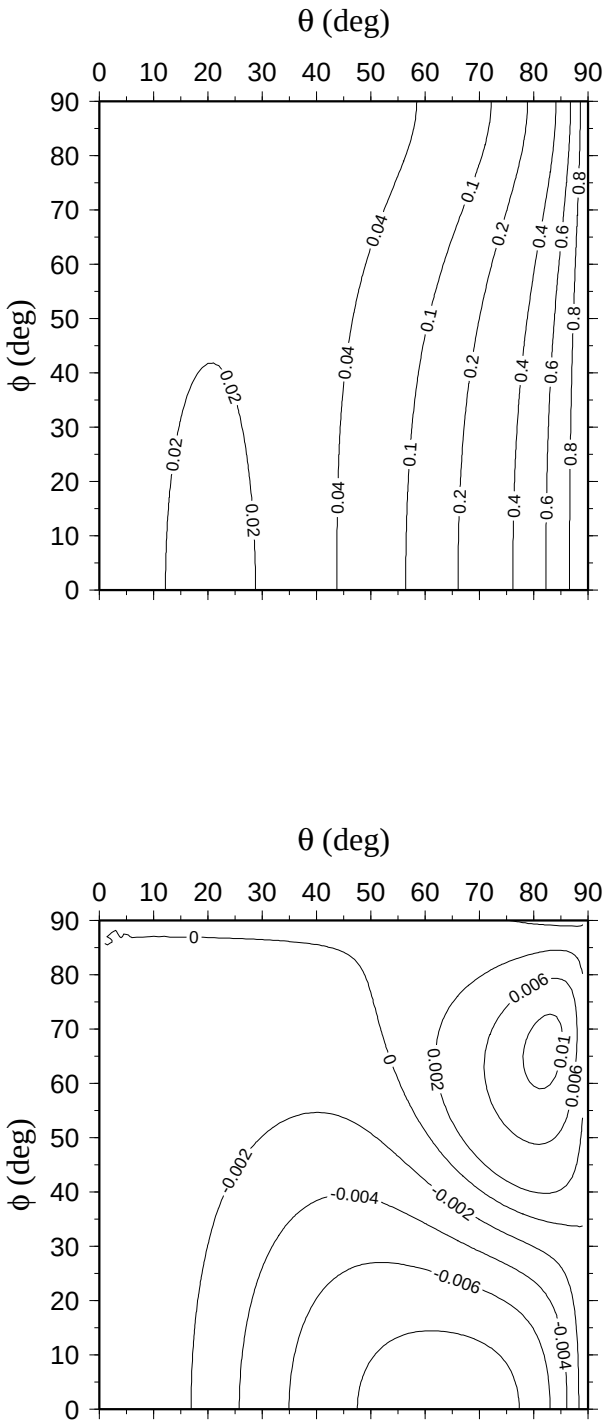

Figure 4: Maps of the moduli of the exact R_{PP} coefficient (top) and of the differences of moduli of the first-order and exact R_{PP} coefficients (bottom) for Model A.

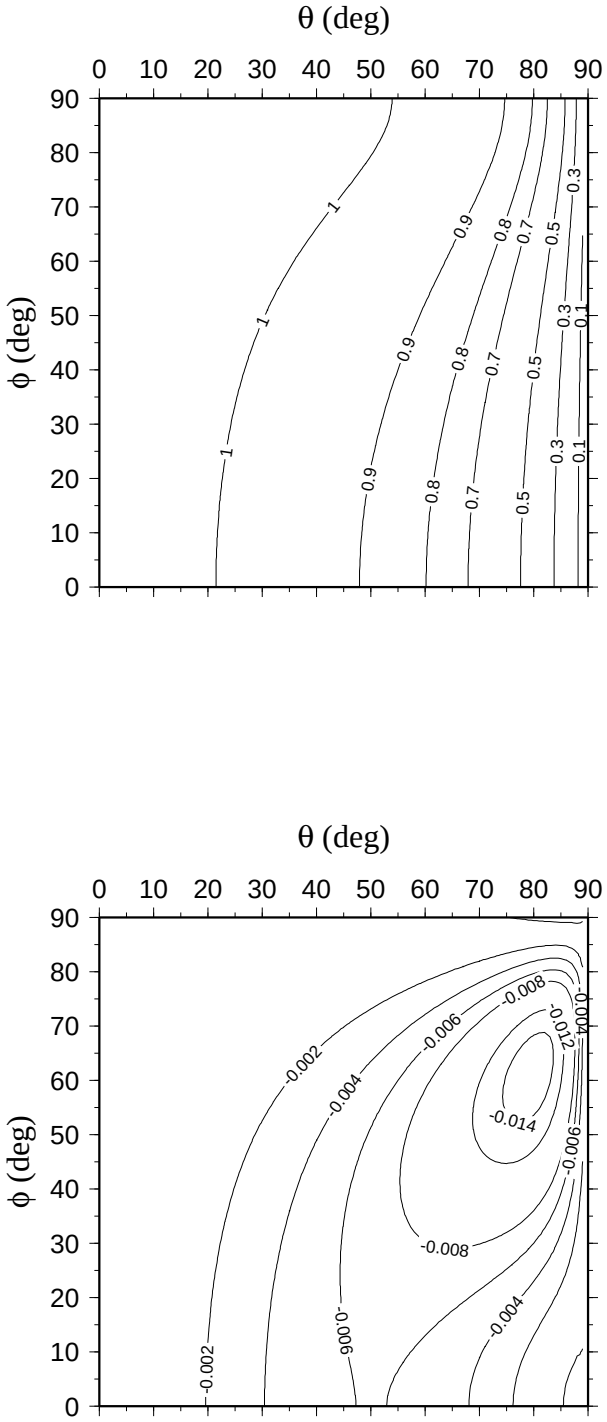

Figure 5: Maps of the moduli of the exact T_{PP} coefficient (top) and of the differences of moduli of the first-order and exact T_{PP} coefficients (bottom) for Model A.

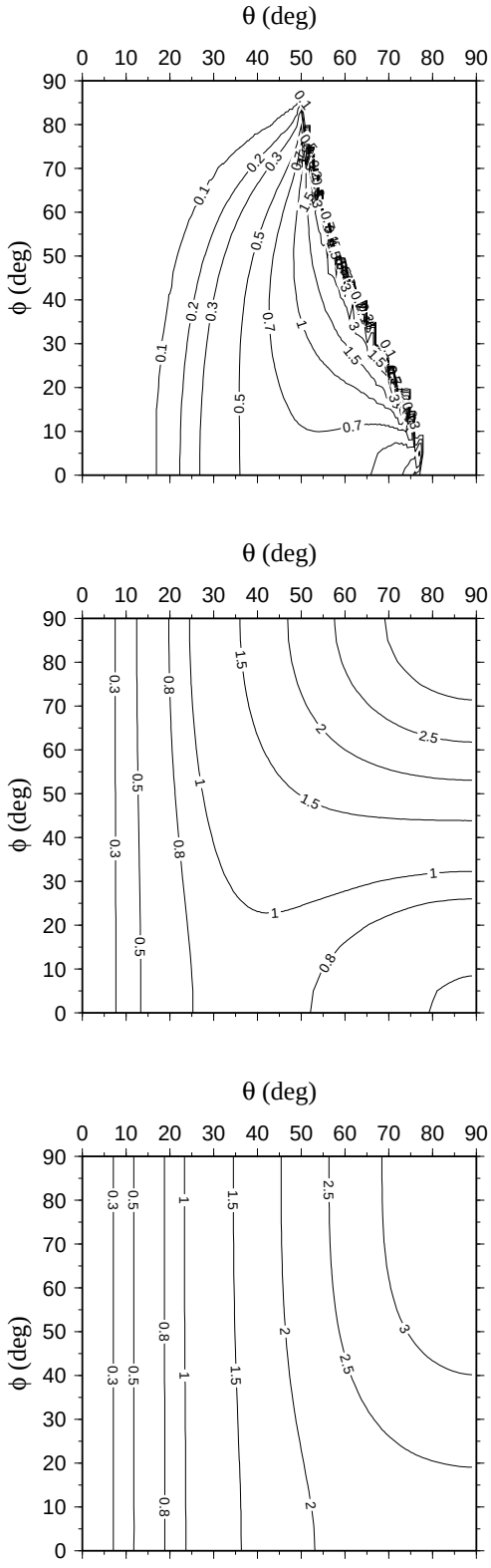

Figure 6: Maps of the angular deviations (in degrees) of approximate and exact slowness vectors of transmitted P (top), S1 (middle) and S2 (bottom) waves for Model B.

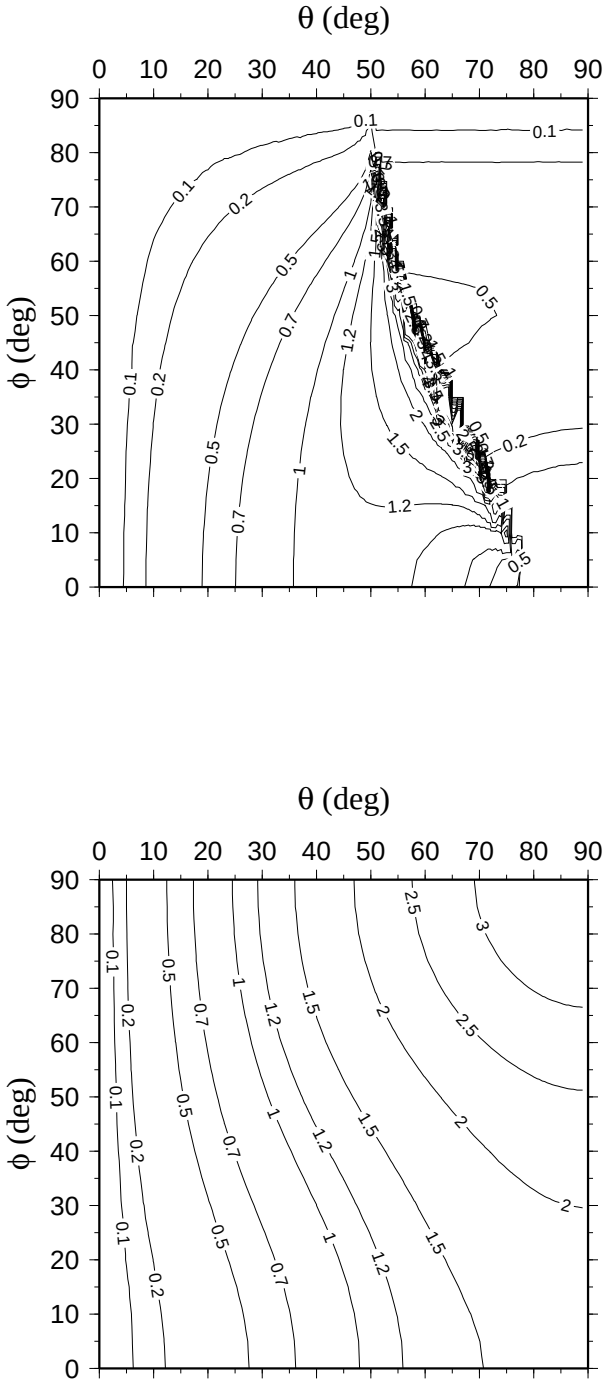

Figure 7: Maps of the angular deviations (in degrees) of approximate and exact polarization vectors of transmitted P (top) and of polarization planes of S (bottom) waves for Model B.

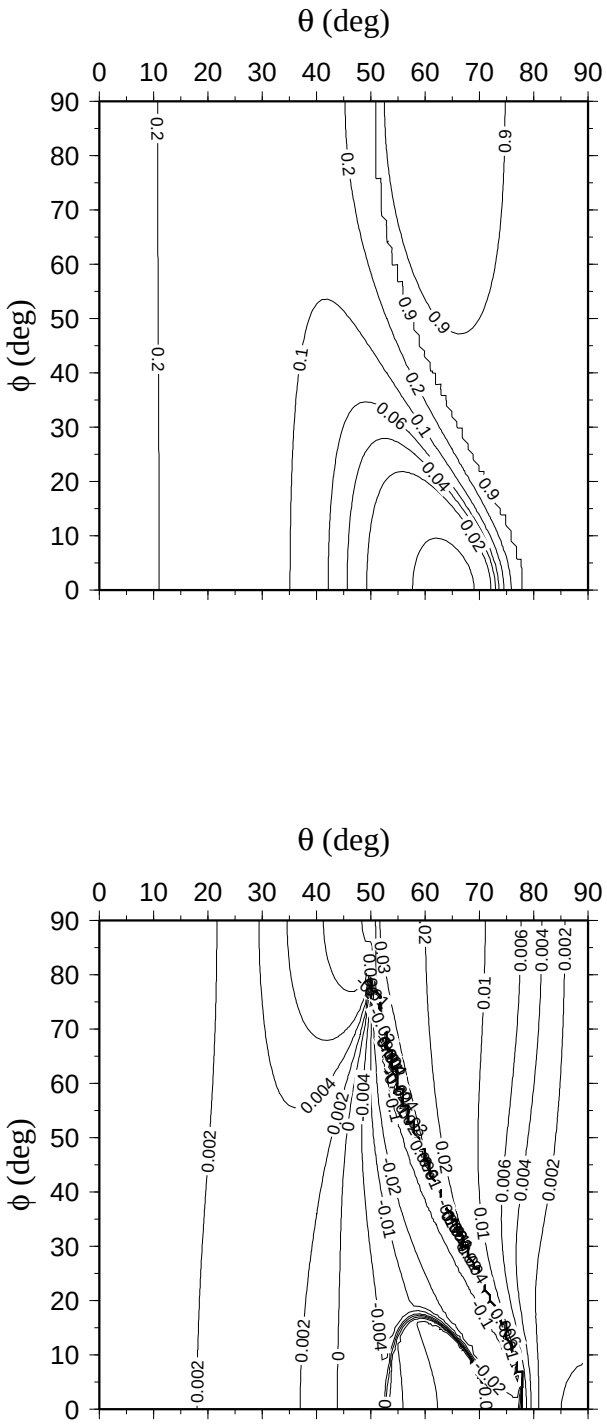

Figure 8: Maps of the moduli of the exact R_{PP} coefficient (top) and of the differences of moduli of the first-order and exact R_{PP} coefficients (bottom) for Model B.

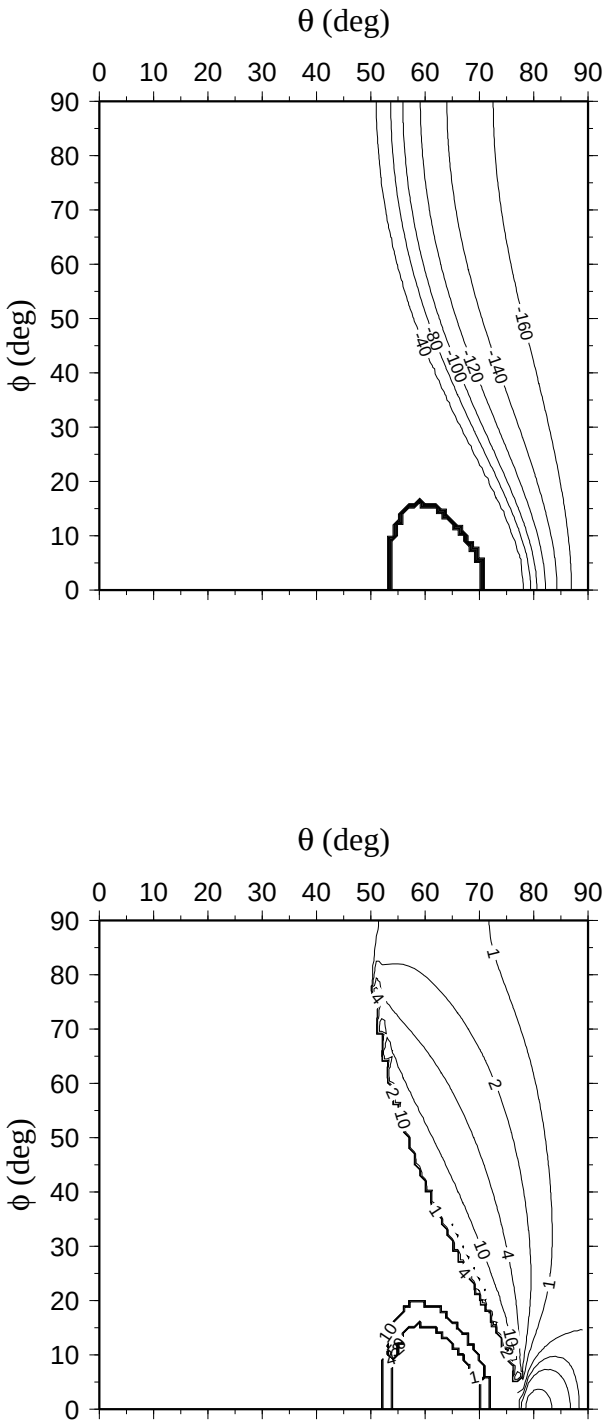

Figure 9: Maps of the phase (in degrees) of the exact R_{PP} coefficient (top) and of the differences of phases of the first-order and exact R_{PP} coefficients (bottom) for Model B.

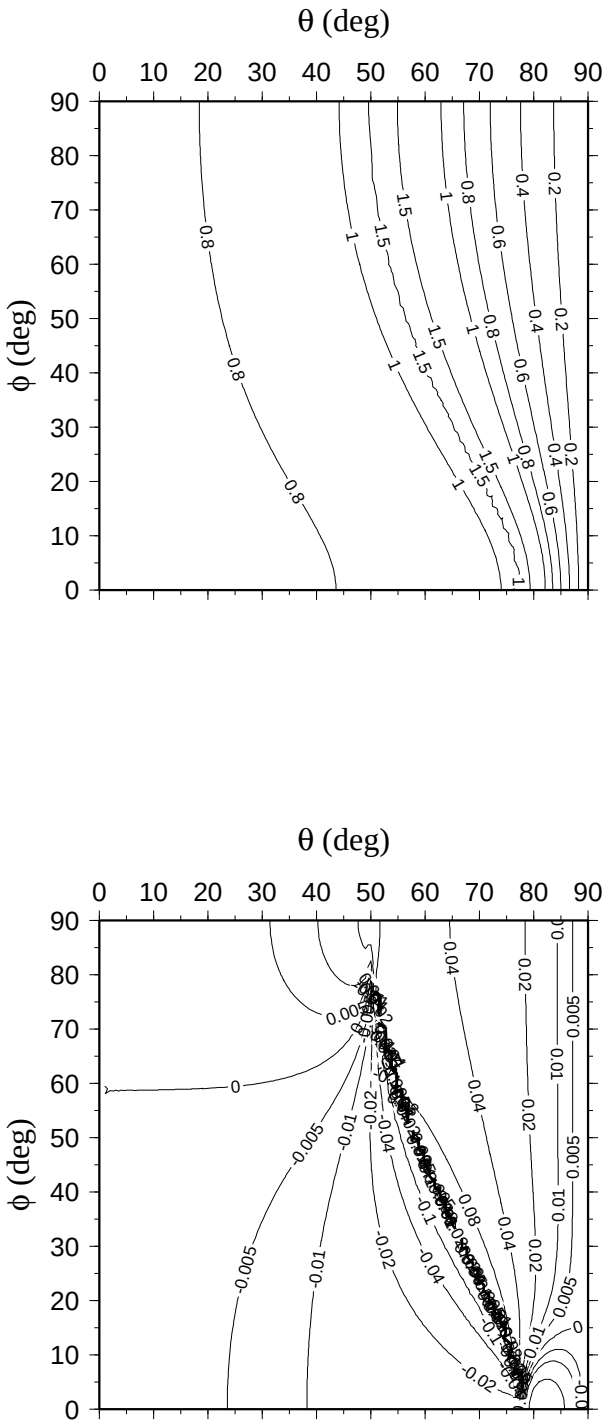

Figure 10: Maps of the moduli of the exact T_{PP} coefficient (top) and of the differences of moduli of the first-order and exact T_{PP} coefficients (bottom) for Model B.

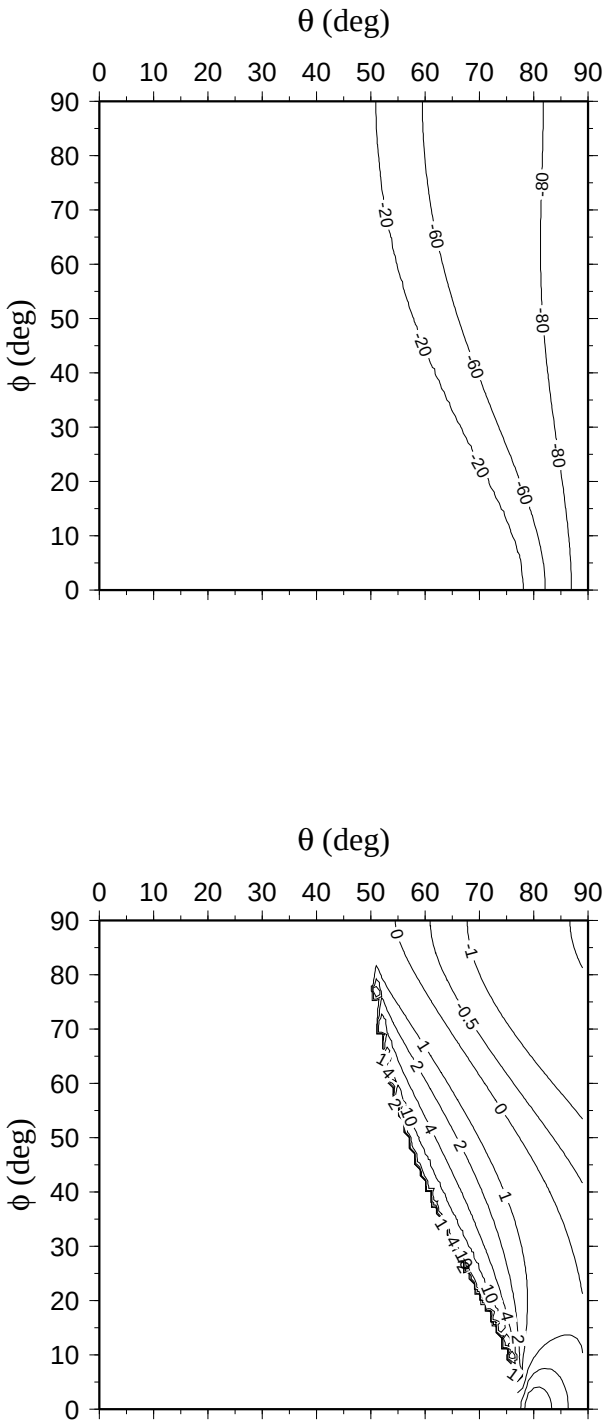

Figure 11: Maps of the phase (in degrees) of the exact T_{PP} coefficient (top) and of the differences of phases of the first-order and exact T_{PP} coefficients (bottom) for Model B.